Band Alignment and the Built-in Potential of Solids

Duk-Hyun Choe,[1] Damien West,[1] and Shengbai Zhang[1,2,*]

[1]*Department of Physics, Applied Physics and Astronomy, Rensselaer Polytechnic Institute, Troy, New York 12180, USA*
[2]*Beijing Computational Science Research Center, 10 East Xibeiwang Road, Beijing 100193, China*

The built-in potential is of central importance to the understanding of many interfacial phenomena because it determines the band alignment at the interface. Despite its importance, its exact sign and magnitude have generally been recognized as ill-defined quantities for more than half a century. Here, we provide a common energy reference of bulk matter which leads to an unambiguous definition of the built-in potential and innate (i.e., bulk) band alignment. Further, we find that the built-in potential is explicitly determined by the bulk properties of the constituent materials when the system is in electronic equilibrium, while the interface plays a role only in the absence of equilibrium. Our quantitative theory enables a unified description of a variety of important properties of interfaces, ranging from work functions to Schottky barriers in electronic devices.

Many intriguing phenomena in nature occur at interfaces. Understanding their behavior is of great interest not only for the study of exciting physics such as highly conducting electrons at the interfaces between insulators [1–4], but also for their direct relevance to virtually all device applications—as coined by Kroemer [5], "the interface is the device." A basic question in these studies is the nature of the charge transfer or variation at the interface that causes the built-in potential between two dissimilar materials. The built-in potential exists at any type of interface [6–8], and it determines a number of fundamental properties in surface or interface science [6–12], such as work functions, electrode potentials, redox potentials, Schottky barriers, and band offsets. Despite more than 50 years of investigation, however, it has not been possible to determine the *exact* sign and magnitude of the built-in potential [7–11]. The absence of a clear understanding of the built-in potential has led to the introduction of numerous terminologies and definitions depending on the field of science and/or purpose. A rigorous definition of the built-in potential is a prerequisite for a quantitative description of many interfacial phenomena and promises a fundamental breakthrough in our understanding of electronic and electrochemical devices [9,11].

A large amount of effort for elucidating the built-in potential can be roughly categorized into two schools of thought. In the first school of thought, the built-in potential is described by the properties of the individual constituent materials. These efforts follow the tradition of building a theoretical framework to understand a complex system from the innate properties of its basic components. Such constructionist approaches have led to numerous failures in interface science, including Schottky barriers and band offsets [9–12]. As a result, in recent years this basic

theoretical approach has been largely neglected [13] in favor of a second school of thought which is typified by detailed quantum mechanical calculations of the specific material interfaces under study. In the second school of thought, the built-in potential is specific to a particular interface. In this regard, the change of the planar averaged charge density $\Delta\bar{\rho}(z)$ is commonly integrated to obtain the built-in potential ψ. However, charge-density-based methods have a fundamental limitation because there is no clear initial basis of comparison for determining $\Delta\bar{\rho}(z)$ and thus have remained a contentious issue [9–11,14–16]. Since both schools of thought have serious limitations, the built-in potential remains an ambiguous property despite its long history of being used to describe the band alignment at interfaces [6–12].

In this work, we present a universal definition of the built-in potential that allows a unified quantitative description of the properties at *any* type of heterojunction interfaces. Based on the theory, we establish a new school of thought on the built-in potential: the built-in potential is determined by the bulk properties of the constituent materials, but only if the system is allowed to reach electronic equilibrium. As pictorially shown in Fig. 1, the key to our finding is identifying a common energy reference among dissimilar *bulk* materials [Fig. 1(c)]. The magnitude of the built-in potential is then explicitly given by the electrostatic potential [Fig. 1(d)], rather than, as generally thought, the charge density. Using metal-metal and metal-semiconductor interfaces as examples, we show that our general theory of built-in potential provides new perspectives into the study of interface science.

We begin by identifying a new reference energy in bulk. For this purpose, we insert vacuum into the bulk in a way that the surfaces have no effect on the average electrostatic
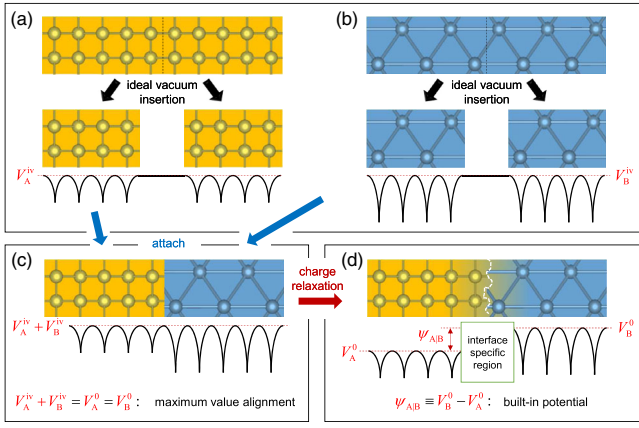
FIG. 1. Schematic diagram for the interface generation and the built-in potential. (a),(b) Illustration for the vacuum insertion within the bulk materials A and B. The ideal vacuum levels (V_A^{iv} and V_B^{iv}) and maximum values (V_A^0 and V_B^0) of the planar averaged electrostatic potentials are denoted as red dashed lines. (c) The ideal A/B interface obtained by attaching the two ideal surfaces. The maximum values are naturally aligned to the same energy before the charge relaxation. (d) The A/B interface after charge relaxation. Here, the built-in potential $\psi_{A|B}$ is well defined even though the boundary between two dissimilar materials is ambiguous.

potential of the nonvacuum regions of the bulk. We term this inserted vacuum the "ideal vacuum," which is a local quantity associated with proximity to the surface. However, it should be distinguished from the "local (or near) vacuum" in the literature [6,9,17], which includes effects due to surface charge and ionic relaxation. The potential relative to the ideal vacuum reflects the bulk property instead of the solid-vacuum interface reflected in the near vacuum associated with work function measurements. Throughout this Letter, we term the surface generated by an ideal vacuum insertion the "ideal surface" [Figs. 2(a) and 2(b)].

The question then is whether the potential of the ideal vacuum V^{iv} can be uniquely defined. As shifts in the local potential of bulk with respect to vacuum are associated with planar surface dipoles, it is sufficient to consider a 1D system here, which is a planar average of the 3D system. One of our key findings is the relationship $V^{iv} = V^0$, where $V^0 = V^0(\hat{n})$ is a maximum value of the *planar averaged* electrostatic potential for a given orientation $\hat{n}$. Consider a periodic system, of length a, which contains a bulk region between z_L and z_R and vacuum elsewhere [Figs. 2(b) and 2(d)]. The dipole moment, $d = \int_0^a z\bar{\rho}(z)dz [= \int_{z_L}^{z_R} z\bar{\rho}(z)dz]$, can be integrated by parts to yield $d = a\bar{E}(a)$, demonstrating that the d must vanish in order for the E field to vanish in the vacuum region. Similarly, for a periodic bulk region, where the boundary of the material is still denoted by z_L and z_R, $d = z_R\bar{E}(z_R) - z_L\bar{E}(z_L) + \bar{\phi}(z_L) - \bar{\phi}(z_R)$, where due to periodicity, $\bar{\phi}(z_L) = \bar{\phi}(z_R)$ and $\bar{E}(z_R) = \bar{E}(z_L)$. Since
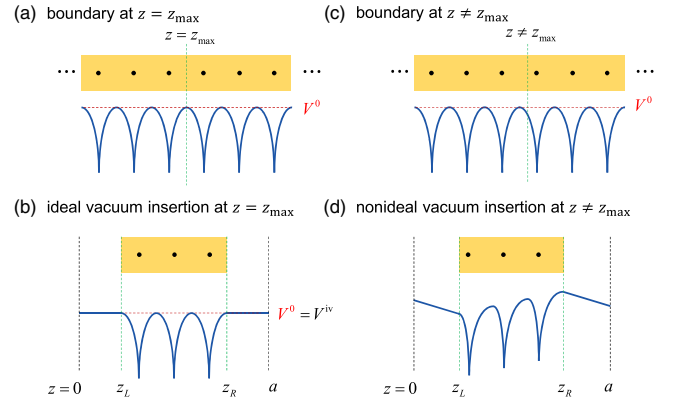

FIG. 2. Electrostatic potential profiles for different choices of surface boundaries. Periodic boundary conditions are considered. Two different boundaries in bulk solid for $z = z_{max}$ and $z \neq z_{max}$ are respectively shown in (a) and (c). The ideal vacuum and nonideal vacuum insertions are respectively illustrated in (b) and (d).

$(z_R - z_L)$ is a physical length that cannot vanish, the dipole moment, $d = (z_R - z_L)\bar{E}(z_L)$, can only vanish when E independently vanishes at the boundaries, $\bar{E}(z_L)[= \bar{E}(z_R)] = 0$. Therefore, in order for the field to vanish in the vacuum, the field at the bulk boundary must also vanish. As $\bar{E} = -\partial_z\bar{\phi}$, the boundary with a vanishing E field corresponds to either a maximum (V^0) or minimum in the planar average electrostatic potential—with the minima being excluded as they would unphysically cut through ions.

It is important to realize that the so-defined V^0 also depends on how the bulk is terminated at the surface. While multiple local maximum levels V^0 can exist in complex materials, such as perovskite oxides [3,4], a unique value of V^0 can always be chosen for a specified surface termination. This is shown schematically for a quaternary polar surface in Figs. 3(a) and 3(b). We further define the "innate work function" of a surface,

$$\varphi^0 = V^0 - E_F, \qquad (1)$$

where E_F is the Fermi level. Both V^0 and E_F are bulk properties, so φ^0 is also a pure bulk property (i.e., innate) and is related to the standard work function φ by the surface dipole S, which accounts for the local potential changes due to charge and ion relaxation, i.e., $\varphi^0 = \varphi - S$. Note that S is a noninnate property which is also affected by the specifics of the interface, e.g., defects, disorder, or surface roughness. As an example, consider the (210) surface depicted in Fig. 3(c). If it is terminated by the dashed line, V^0 is aligned with the ideal vacuum. Because of the roughness, however, the material above the dashed line can have an associated dipole contributing to S.

Next, we imagine the interface formation in two steps: (i) the creation of an ideal A/B interface, which consists of two ideal surfaces of material A and B [Figs. 1(a)–1(c)], and (ii) allowing the electrons and ions to relax to find the
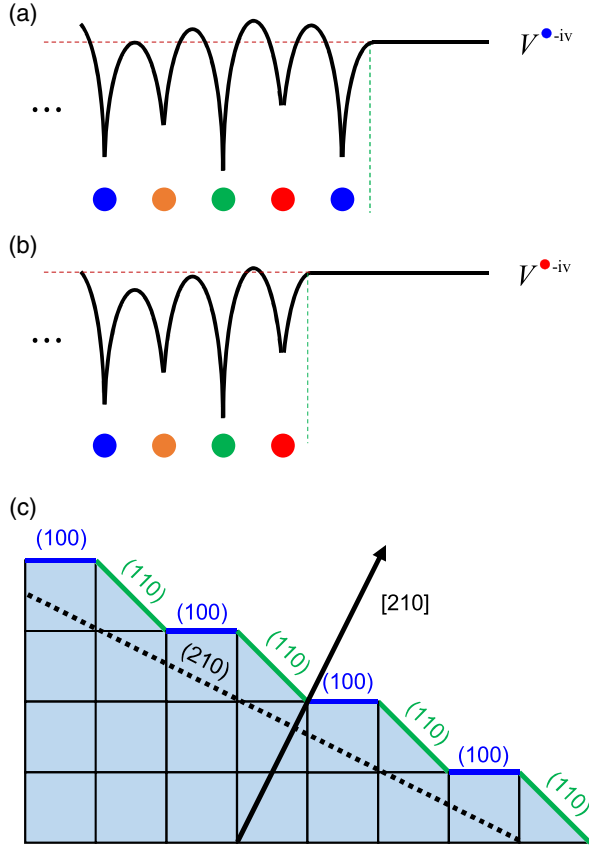
FIG. 3. Complex surface terminations. (a),(b) Electrostatic potential profiles of ideal surfaces for a material consisting of four atoms in the unit cell. The four atoms are denoted as blue, yellow, green, and red filled circles, respectively. The ideal surfaces for blue-atom- (blue dots) and red-atom- (red dots) terminated cases are shown in (a) and (b), respectively. (c) An example of a (210) surface that contains (100) and (110) facets.

ground state [Fig. 1(d)]. Comparison of the average electrostatic potential of the systems in the above two steps yields a potential shift arising from the interfacial charge transfer, which is the very definition of the built-in potential. We find from Fig. 1(d) that the built-in potential is simply defined as the difference between V^0 in bulk regions of the two materials:

$$\psi_{A|B} = V_B^0 - V_A^0. \qquad (2)$$

This happens because V_A^0 and V_B^0 for the two ideal surfaces [Figs. 1 and 2(a)] are aligned to the same energy before the charge transfer, which can be understood based on the principal of linear superposition of potentials [9]: consider, e.g., the superimposed $A + B$ system with a vacuum region between A and B, the potential at the boundary of material A, which was previously V_A^{iv} becomes $V_A^{\text{iv}} + V_B^{\text{iv}}$, due to the addition of a constant potential (V_B^{iv}) introduced by system B in this region. Similarly, the potential at the boundary of material B also becomes

$V_A^{\text{iv}} + V_B^{\text{iv}}$. Therefore, irrespective of an arbitrary constant added to either potential, the alignment shown in Fig. 1(c) ($V_A^0 = V_B^0$) is true.

An important consequence of Eq. (2) is that in *any* type of heterojunction in electronic equilibrium, the built-in potential $\psi_{A|B}$ is determined entirely from the bulk properties of the material A and B. In such a case, the interface charge transfer takes place in order to align the Fermi level; i.e., $E_{F,A} = E_{F,B}$. This combined with Eqs. (1) and (2) yields

$$\psi_{A|B} = (\varphi^0 + E_F)_B - (\varphi^0 + E_F)_A = \varphi_B^0 - \varphi_A^0. \qquad (3)$$

The innate properties of the individual constituent materials therefore dictate the built-in potential at the interface under equilibrium, irrespective of complex interfacial details. In other words, the built-in potential is subject to properties of the interface *only* when the system is not allowed to reach equilibrium.

To illustrate these definitions and conclusions we performed density functional theory (DFT) calculations on 12 different M/M heterojunction interfaces: Al/Ag, Al/Au, Ag/Au, and Ni/Cu heterojunctions with interfaces along (100), (110), and (111). In each case, we calculate ψ by the difference in V^0 through DFT-relaxed heterostructures [Eq. (2)]. These values are then compared to the value of ψ calculated from the innate work functions via Eq. (3). We see from Table I essentially exact agreement, which is a direct consequence of Poisson's equation. As a comparison, we consider the work function difference ($\varphi_B - \varphi_A$) as $\psi_{A|B}$ and find that it gives at best a crude estimate of the built-in potential. The inability of the φ-based approach can be understood as it includes charge relaxation into the vacuum, not present at the interface.

TABLE I. Calculated built-in potentials at the interfaces between two metals, based on $V_B^0 - V_A^0$, $\varphi_B^0 - \varphi_A^0$, and $\varphi_B - \varphi_A$. Our DFT calculations were performed using Perdew-Burke-Ernzerhof (PBE) exchange-correlation functional [18] and the projector augmented wave (PAW) pseudopotentials [19], as implemented in the VASP code [20]. Ionic relaxations are not considered for simplicity.

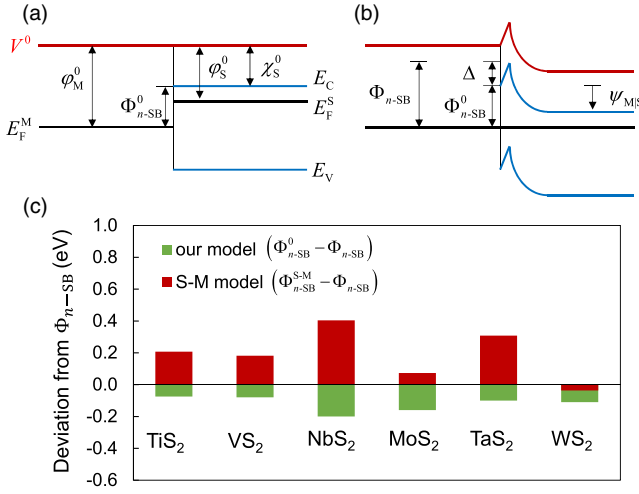| Interfaces		$V_B^0 - V_A^0$	$\varphi_B^0 - \varphi_A^0$	$\varphi_B - \varphi_A$
Al/Ag	(111)	0.988	1.003	0.364
	(110)	−0.030	−0.039	−0.088
	(100)	0.924	0.914	−0.019
Al/Au	(111)	0.569	0.575	1.096
	(110)	−1.949	−1.955	0.899
	(100)	0.121	0.136	0.821
Ag/Au	(111)	−0.393	−0.391	0.731
	(110)	−1.843	−1.843	0.817
	(100)	−0.743	−0.720	0.847
Ni/Cu	(111)	−0.627	−0.631	−0.334
	(110)	−0.490	−0.505	−0.214
	(100)	−0.576	−0.574	−0.408

FIG. 4. Schematic band diagram for metal-semiconductor heterojunctions. (a) Depicts the innate alignment of the ideal M-S interface for the case of an n-doped semiconductor without any electronic or ionic relaxation. The common energy reference V^0 is denoted by the red solid lines. The Fermi levels and the band edges are denoted as solid black and blue lines, respectively. As there is no relaxation, the Fermi levels are not aligned. (b) The M-S interfaces after allowing for full ionic and electronic relaxations. (c) Comparison between Schottky-Mott model ($\Phi_{n\text{-SB}}^{\text{SM}}$) and our model ($\Phi_{n\text{-SB}}^{0}$) for $1T$-MS_2/$2H$-MoS_2 stacked heterostructures with $M = $ (Ti, V, Nb, Mo, Ta, W). We consider 8 layers of $1T$ transition metal dichalcogenides stacked with 8 layers of $2H$-MoS_2 in the supercell calculations. We fix the in-plane lattice constant to the experimental value of $2H$-MoS_2 ($a = 3.16$ Å) and obtained the optimized bulk structure of $1T$ transition metal dichalcogenides by relaxing the out-of-plane lattice constant. We considered the PBE + D3 method for van der Waals interaction.

Next, we consider metal-semiconductor (M-S) interfaces. Figure 4(a) illustrates the innate band alignment of the M-S junctions with n-doped semiconductors by aligning V^0, which can be obtained purely from bulk calculations without slab or heterojunction geometry considerations. After charge relaxation [Fig. 4(b)], a dipole at the interface is developed. Since the dipole is the sole source of the built-in potential, charge transfer effects at the immediate interface, such as chemical bonding, defects, and disorder, can only contribute higher order electrostatic terms (quadrupole, octupole, etc.), leading to the development of a potential barrier (or well) Δ in the semiconductor region in Fig. 4(b). An important advantage of introducing the innate band alignment is that it provides a clear distinction between innate and noninnate (i.e., interfacial) properties of heterojunctions, which has long been ambiguous [9–12, 14–16,21–28]. In the current case, n-type Schottky barrier (SB) ($\Phi_{n\text{-SB}}$) is the barrier electrons need to overcome in order to transport from metal to semiconductor. In analogy to the Schottky-Mott (SM) model [29,30], we can define an innate n-type SB $\Phi_{n\text{-SB}}^{0} = \varphi_M^0 - \chi_S^0$, where φ_M^0 is the innate

work function of metal and χ_S^0 is the innate electron affinity of semiconductor [Fig. 4(a)], such that $\Phi_{n\text{-SB}}$ is decomposed into $\Phi_{n\text{-SB}}^0$ and Δ [i.e., $\Phi_{n\text{-SB}} = \Phi_{n\text{-SB}}^0 + \Delta$ in Fig. 4(b)].

When $\Delta \approx 0$, e.g., in van der Waals (vdW) systems [31–33], one can expect that the SBs can be reasonably well described by innate properties. Figure 4(c) shows the SBs for several stacked transition metal dichalcogenide heterostructures. It is found that these innate barriers agree reasonably well with the SBs from full heterostructure calculations and a systematic improvement over the SM limit is obtained. This improvement is also evident from a direct comparison to recent experiments [34–36]. The innate n-type SB of the $2H$-$MoTe_2$/$1T'$-$MoTe_2$ junction is calculated to be 0.01 eV, qualitatively different from the SB in the SM limit of 0.37 eV, but in good agreement with the experiment reporting an n-type Ohmic contact [34]. Additionally, the innate p-type SB of the stacked $2H$-$NbSe_2$/$2H$-WSe_2 is calculated to be 0.03 eV, qualitatively different from the SB in the SM limit of 0.40 eV, but in good agreement with the experimental value of 0.05 eV [35,36].

In summary, we have presented a rigorous definition of the innate band alignment between solids, which allows for calculation of the surface dipole and built-in potential. It enables a clear distinction between innate and noninnate properties at interfaces, and we have used it to define the innate work function (φ^0), band offset, and Schottky barrier (Φ_{SB}^0)—which can be calculated without explicit consideration of the interface. First-principles calculations show that in the case of weak interfacial interaction, such as vdW interfaces, the SB is well described by Φ_{SB}^0, which yields systematic improvement over the Schottky-Mott limit. Beyond the interfacial physics, the insight into the common energy reference of bulk solids provides clues for understanding the long-standing problem of defining an average electrostatic potential of infinitely large systems, enabling the determination of a number of bulk properties: e.g., deformation potentials [37,38], universal electronic behaviors of materials [27,28,39], and formation energies of charged defects [40,41].

*Corresponding author.
zhangs9@rpi.edu.

[1] J. E. Moore, Nature (London) **464**, 194 (2010).
[2] M. Z. Hasan and C. L. Kane, Rev. Mod. Phys. **82**, 3045 (2010).

[3] J. Mannhart and D. G. Schlom, Science **327**, 1607 (2010).

[4] H. Y. Hwang, Y. Iwasa, M. Kawasaki, B. Keimer, N. Nagaosa, and Y. Tokura, Nat. Mater. **11**, 103 (2012).

[5] H. Kroemer, Rev. Mod. Phys. **73**, 783 (2001).

[6] S. M. Sze and K. K. Ng, *Physics of Semiconductor Devices*, 3rd ed. (Wiley, Hoboken, NJ, 2007).

[7] *Fundamentals of Electrochemistry*, 2nd ed. V. S. Bagotsky (Wiley, Hoboken, NJ, 2005).

[8] A. J. Bard and L. R. Faulkner, *Electrochemical Methods: Fundamentals and Applications*, 2nd ed. (Wiley, New York, 2001).

[9] R. T. Tung, Appl. Phys. Rev. **1**, 011304 (2014).

[10] S. Baroni, R. Resta, A. Baldereschi, and M. Peressi, Can we tune the band offset at semiconductor heterojunctions?, in *Spectroscopy of Semiconductor Microstructures*, edited by G. Fasol *et al.* (Springer, New York, 1989), pp. 251–271.

[11] A. Franciosi and C. G. Van de Walle, Surf. Sci. Rep. **25**, 1 (1996).

[12] J. Robertson, J. Vac. Sci. Technol. A **31**, 050821 (2013).

[13] P. W. Anderson, Science **177**, 393 (1972).

[14] C. G. Van de Walle and R. M. Martin, Phys. Rev. B **35**, 8154 (1987).

[15] D. M. Bylander and L. Kleinman, Phys. Rev. Lett. **59**, 2091 (1987).

[16] A. Baldereschi, S. Baroni, and R. Resta, Phys. Rev. Lett. **61**, 734 (1988).

[17] D. Cahen and A. Kahn, Adv. Mater. **15**, 271 (2003).

[18] J. P. Perdew, K. Burke, and M. Ernzerhof, Phys. Rev. Lett. **77**, 3865 (1996).

[19] P. E. Blöchl, Phys. Rev. B **50**, 17953 (1994).

[20] G. Kresse and J. Furthmüller, Phys. Rev. B **54**, 11169 (1996).

[21] J. Tersoff, Phys. Rev. B **30**, 4874 (1984).

[22] S. B. Zhang, M. L. Cohen, and S. G. Louie, Phys. Rev. B **32**, 3955 (1985).

[23] S. B. Zhang, M. L. Cohen, and S. G. Louie, Phys. Rev. B **34**, 768 (1986).

[24] S.-H. Wei and A. Zunger, Phys. Rev. Lett. **59**, 144 (1987).

[25] R. T. Tung, Phys. Rev. Lett. **84**, 6078 (2000).

[26] R. T. Tung, Phys. Rev. B **64**, 205310 (2001).

[27] Y.-H. Li, A. Walsh, S. Chen, W.-J. Yin, J.-H. Yang, J. Li, J. L. F. Da Silva, X. G. Gong, and S.-H. Wei, Appl. Phys. Lett. **94**, 212109 (2009).

[28] C. G. Van de Walle and J. Neugebauer, Nature (London) **423**, 626 (2003).

[29] W. Schottky, Z. Phys. **113**, 367 (1939).

[30] N. F. Mott, Proc. R. Soc. A **171**, 27 (1939).

[31] A. K. Geim and I. V. Grigorieva, Nature (London) **499**, 419 (2013).

[32] K. S. Novoselov, A. Mishchenko, A. Carvalho, and A. H. Castro Neto, Science **353**, aac9439 (2016).

[33] Y. Liu, P. Stradins, and S.-H. Wei, Sci. Adv. **2**, e1600069 (2016).

[34] S. Cho *et al.*, Science **349**, 625 (2015).

[35] J. Guan, H.-J. Chuang, Z. Zhou, and D. Tománek, ACS Nano **11**, 3904 (2017).

[36] Y. Sata, R. Moriya, S. Masubuchi, K. Watanabe, T. Taniguchi, and T. Machida, Jpn. J. Appl. Phys. **56**, 04CK09 (2017).

[37] J. Bardeen and W. Shockley, Phys. Rev. **80**, 72 (1950).

[38] C. G. Van de Walle and R. M. Martin, Phys. Rev. Lett. **62**, 2028 (1989).

[39] S. B. Zhang, S.-H. Wei, and A. Zunger, J. Appl. Phys. **83**, 3192 (1998).

[40] S. B. Zhang and J. E. Northrup, Phys. Rev. Lett. **67**, 2339 (1991).

[41] C. Freysoldt, B. Grabowski, T. Hickel, J. Neugebauer, G. Kresse, A. Janotti, and C. G. Van de Walle, Rev. Mod. Phys. **86**, 253 (2014).